

Integrin $\alpha_5\beta_1$ -targeted [Cu]CuS Nanoparticles for PET/ CT Imaging and Photothermal Ablation Therapy

Lili Cui, Chiyi Xiong, Min Zhou, Sixiang Shi, Diana S-L Chow, and Chun Li

Bioconjugate Chem., **Just Accepted Manuscript** • DOI: 10.1021/acs.bioconjchem.8b00690 • Publication Date (Web): 08 Nov 2018

Downloaded from <http://pubs.acs.org> on November 8, 2018

Just Accepted

“Just Accepted” manuscripts have been peer-reviewed and accepted for publication. They are posted online prior to technical editing, formatting for publication and author proofing. The American Chemical Society provides “Just Accepted” as a service to the research community to expedite the dissemination of scientific material as soon as possible after acceptance. “Just Accepted” manuscripts appear in full in PDF format accompanied by an HTML abstract. “Just Accepted” manuscripts have been fully peer reviewed, but should not be considered the official version of record. They are citable by the Digital Object Identifier (DOI®). “Just Accepted” is an optional service offered to authors. Therefore, the “Just Accepted” Web site may not include all articles that will be published in the journal. After a manuscript is technically edited and formatted, it will be removed from the “Just Accepted” Web site and published as an ASAP article. Note that technical editing may introduce minor changes to the manuscript text and/or graphics which could affect content, and all legal disclaimers and ethical guidelines that apply to the journal pertain. ACS cannot be held responsible for errors or consequences arising from the use of information contained in these “Just Accepted” manuscripts.

1
2
3 **Integrin $\alpha v \beta 3$ -targeted [^{64}Cu]CuS Nanoparticles for PET/CT Imaging and Photothermal**
4
5 **Ablation Therapy**
6
7
8
9

10 Lili Cui^{1#}, Chiyi Xiong^{2#}, Min Zhou^{2,3}, Sixiang Shi², Diana S-L. Chow^{1*}, and Chun Li^{2*}
11
12
13

14 ¹Department of Pharmacological and Pharmaceutical Sciences, College of Pharmacy, University
15 of Houston, Houston, TX 77024, USA
16
17

18 ²Department of Cancer Systems Imaging, The University of Texas MD Anderson Cancer Center,
19 Houston, TX 77054-1907, USA
20
21

22 ³Institute of Translational Medicine, School of Medicine, Zhejiang University, Hangzhou, 310029,
23 China
24
25

26 #These authors (Lili Cui, Chiyi Xiong) contributed equally.
27
28

29 *Corresponding authors:
30
31

32 Chun Li, Department of Cancer Systems Imaging–Unit 1907, The University of Texas MD
33 Anderson Cancer Center, 1881 East Road, Houston, TX 77030
34
35

36 E-mail: cli@mdanderson.org
37
38

39 Diana S-L. Chow, Department of Pharmacological and Pharmaceutical Sciences, College of
40 Pharmacy, University of Houston, Houston, Texas 77204
41
42

43 Email: phar33@central.uh.edu
44
45
46
47
48
49
50
51
52
53
54
55
56
57
58
59
60

Abstract

Copper sulfide (CuS) nanoparticles have been considered one of the most clinical relevant nanosystems because of their straightforward chemistry, small particle size, low toxicity, and intrinsic theranostic characteristics. In our previous studies, radioactive [^{64}Cu]CuS nanoparticles were successfully developed to be used as efficient radiotracers for positron emission tomography and for photothermal ablation therapy of cancer cells using near-infrared laser irradiation. However, the major challenge of CuS nanoparticles as a theranostic platform is the lack of a means for effective targeted delivery to the tumor site. To overcome this challenge, we designed and synthesized angiogenesis-targeting [^{64}Cu]CuS nanoparticles, which are coupled with cyclic RGDfK peptide [c(RGDfK)] through polyethylene glycol (PEG) linkers using click chemistry. In assessing their tumor-targeting efficacy, we found that the tumor uptakes of [^{64}Cu]CuS-PEG-c(RGDfK) nanoparticles at 24 h after intravenous injection were significantly greater ($8.6\% \pm 1.4\%$ injected dose/gram of tissue) than those of nontargeted [^{64}Cu]CuS-PEG nanoparticles ($4.3\% \pm 1.2\%$ injected dose/gram of tissue, $p < 0.05$). Irradiation of tumors in mice administered [^{64}Cu]CuS-PEG-c(RGDfK) nanoparticles induced 98.7% necrotic areas. In contrast, irradiation of tumors in mice administered non-targeted CuS-PEG nanoparticles induced 59% necrotic areas ($p < 0.05$). The angiogenesis-targeting [^{64}Cu]CuS nanoparticles may serve as a promising platform for image-guided ablation therapy with high efficacy and minimal side effects in future clinical translation of this novel class of multifunctional nanomaterials.

1
2
3 Because of their distinctive physicochemical properties, nanoparticles offer a unique
4 opportunity for combining cancer diagnosis and therapy in a single system, i.e., theranostics.¹
5
6 Copper sulfide (CuS) nanoparticles are synthesized in one straightforward step, displaying small
7
8 particle size (5-20 nm in diameter), low toxicity, and intrinsic theranostic properties. Moreover,
9
10 CuS nanoparticles are amenable without surface chemistry changes to ⁶⁴Cu labeling for positron
11
12 emission tomography (PET) imaging and radiotherapy; they also show promise as contrast agents
13
14 for photoacoustic imaging and as photothermal coupling agents for photothermal ablation (PTA)
15
16 therapy owing to their strong absorption in the near-infrared (NIR) region.²⁻⁷ For example, CuS
17
18 nanoparticles have been intrinsically labeled with ⁶⁴Cu for PET imaging and employed for
19
20 combined radiotherapy and PTA, taking advantage of the ionizing radiation from β particles
21
22 emitted from ⁶⁴Cu and the photothermal conversion property of the CuS nanoparticles.^{8, 9} The
23
24 quantitative imaging provided by these nanoparticles was excellent, while the synergistic
25
26 radiotherapy/PTA completely eliminated the primary tumor and prevented potential tumor
27
28 metastasis without any apparent toxicity.
29
30
31
32
33
34

35 Although CuS nanoparticles were proven to be an excellent platform for accurate imaging
36
37 and effective therapy, the major challenge is the lack of a means for efficient delivery to the tumor
38
39 site.¹⁰ In some cases, intratumoral injection has been used to ensure sufficient tumor retention of
40
41 ⁶⁴Cu-labeled CuS ([⁶⁴Cu]CuS) nanoparticles for effective radiotherapy. However, intratumoral
42
43 injection is not suitable for treating metastatic lesions or tumors located in sites inaccessible to
44
45 minimally invasive interventions. While systemic administration can lead to passive targeting and
46
47 tumor accumulation of CuS nanoparticles through the enhanced permeability and retention effect,
48
49 the efficiency of passive targeting is highly variable and is influenced by a number of factors, such
50
51
52
53
54
55
56
57
58
59
60

1
2
3 as particle size, surface characteristics, and degree of angiogenesis and permeability of tumor
4
5 blood vessels.¹¹
6

7
8 It is highly desirable that CuS nanoparticles are selectively delivered to tumor sites through
9
10 active targeting mechanisms to improve therapeutic outcome.¹ Among the strategies for active
11
12 targeting, targeting angiogenic blood vessels is especially attractive because this approach does
13
14 not require nanoparticles entering the extravascular fluid space, a rate-limiting, inefficient process
15
16 for nanoparticle delivery. Angiogenesis is required for supporting tumor growth by ensuring
17
18 continuous supply of nutrients and oxygen.¹² As the cell adhesion molecule integrin $\alpha v \beta 3$ is
19
20 overexpressed in angiogenic blood vessels.¹³ It specifically binds to stroma proteins containing
21
22 the tripeptide motif arginine-glycine-aspartic acid (RGD), such as fibrinogen, vitronectin,
23
24 thrombospondin, and osteopontin.^{14, 15} Cyclic pentapeptides that have a relatively high and specific
25
26 affinity for the RGD sequence of the $\alpha v \beta 3$ integrin have been used to improve imaging contrast
27
28 with imaging probes and to enhance delivery efficiency of nanoparticles.¹⁶⁻¹⁸
29
30
31

32
33 In previous studies, chelator-free [⁶⁴Cu]CuS nanoparticles synthesized rapidly by a simple
34
35 process were shown to possess high radiolabeling stability and high specific activity. Chemically,
36
37 ⁶⁴Cu is the same as its naturally abundant ^{nat}Cu used to build CuS nanoparticles. As such, no
38
39 radiometal chelator is required for radiolabeling of CuS nanoparticles; [⁶⁴Cu]CuS nanoparticles
40
41 synthesized by doping CuS with tracer amount of ⁶⁴Cu were shown to be stable and used in both
42
43 PET u and a PTA therapy.⁵ We hypothesized, therefore, that c(RGDfK)-tagged [⁶⁴Cu]CuS
44
45 nanoparticles can increase the tumor-targeting efficiency over untagged nanoparticles and mediate
46
47 an effective antitumor effect. In this work, we report the first click-chemistry-assisted synthesis
48
49 for the introduction of peptides to the surface to the class of CuS nanoparticles, their
50
51
52
53
54
55
56
57
58
59
60

1
2
3 physicochemical characterization and specific cellular binding *in vitro*, and *in vivo* uptake and
4
5 therapeutic effect in tumor xenograft models.
6
7
8
9

10 RESULTS

11
12 **Synthesis and characterization of CuS-PEG-c(RGDfK) nanoparticles.** The reaction
13
14 scheme for the introduction of c(RGDfK) peptide to CuS-polyethylene glycol (PEG) nanoparticles
15
16 is shown in **Figure 1**. The c(RGDfK) peptide was synthesized by standard Fmoc solid-phase
17
18 strategy. The structures of the starting, intermediate, and final products were confirmed by ¹H
19
20 NMR (500 MHz) (**Figure S1-S4**). The side chain amine group on Lys was then reacted with 4-
21
22 pentynoic acid to introduce the alkyne functional group, which was confirmed by liquid
23
24 chromatography/mass spectrometry (LC/MS; mass calculated for c(RGDfK): 603.68, found:
25
26 [M+H⁺] = 604.33; mass calculated for 4-pentynoic acid–modified c(RGDfK): 683.69, found:
27
28 [M+H⁺] = 684.34).^{19, 20}
29
30
31
32
33
34
35
36
37
38
39
40
41
42
43
44
45
46
47
48
49
50
51
52
53
54
55
56
57
58
59
60

Figure 1

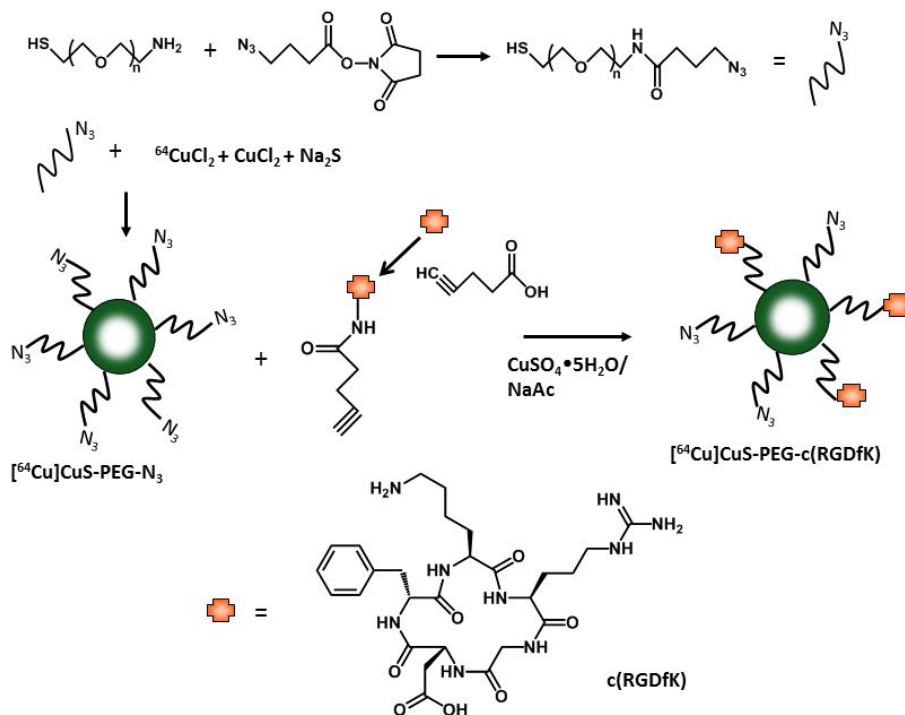


Figure 1. Schematic illustration of the synthesis of $[^{64}\text{Cu}]\text{CuS-PEG-c(RGDfK)}$ nanoparticles.

CuS-PEG- N_3 nanoparticles were rapidly synthesized from CuCl_2 and Na_2S in the presence of thiol-PEG-azide in water. The reaction proceeded at 90°C for 15 min. ^1H NMR spectra showed a peak at 3.6 ppm characteristic of $\text{CH}_2\text{CH}_2\text{O}$ repeating units in PEG, suggesting that the CuS nanoparticles were coated by thiol-PEG- N_3 (**Figure S5a**). The alkyne-modified c(RGDfK) was attached to the CuS-PEG- N_3 nanoparticles through azide-alkyne click chemistry in aqueous phase in the presence of copper catalyst.²¹ Analysis of amino acid composition in the resulting CuS-PEG-c(RGDfK) nanoparticles showed that the molar ratio of RGD peptide to PEG chains on the

1
2
3 surface of the nanoparticles could be readily controlled by controlling the feeding ratio of alkyne-
4 modified c(RGDfK) and PEG-N₃ (**Table S1**).

5
6
7
8 The maximum absorption wavelengths for both CuS-PEG and CuS-PEG-c(RGDfK)
9 nanoparticles were ~970 nm (**Figure S5b**), confirming that the modification with c(RGDfK)
10 peptide did not significantly change the optical property of PEG-CuS nanoparticles.⁵ The
11 hydrodynamic sizes of the CuS-PEG and CuS-PEG-c(RGDfK) nanoparticles were 42±0.6 nm and
12 49.7±0.4 nm, respectively. The zeta potential of CuS-PEG-c(RGDfK) nanoparticles (-11 mV) was
13 less negative than that of PEG-CuS nanoparticles (-24 mV) because of the positive charge in the
14 guanidinium group of the arginine in c(RGDfK) (**Figure S5c and S5d**), suggesting successful
15 peptide conjugation. TEM images confirmed that the diameters of both CuS-PEG and CuS-PEG-
16 c(RGDfK) were less than 50 nm, and were spherical and irregular in shape (**Fig. S5e**). The yields
17 of peptide molecules conjugated to the surface of CuS-PEG nanoparticles by click chemistry was
18 87% when the molar ratio of peptide-to-PEG was 0.08:1. The yield decreased to 60% when the
19 peptide-to-PEG molar ratio was increased to 0.6:1 (**Table S1**).

20
21
22
23
24
25
26
27
28
29
30
31
32
33
34
35
36 To examine the photothermal effect in aqueous solution after peptide modification of the
37 nanoparticles, we compared the photothermal effect of CuS-PEG-c(RGDfK) nanoparticles with
38 that of CuS-PEG nanoparticles using two different laser power levels. The temperature was
39 elevated to 46.1°C and 45.2°C at 2 OD (optical density) for CuS-PEG and CuS-PEG-c(RGDfK)
40 nanoparticles, respectively, at a laser power density of 1 W/cm². The maximum temperature
41 increased to 36.9°C and 35.6°C for CuS-PEG and CuS-PEG-c(RGDfK) nanoparticles,
42 respectively, at a laser power density of 0.5 W/cm² (**Figure 2a**). The photothermal effect in
43 aqueous solution did not differ significantly for the two nanoparticles. To assess the photothermal
44 effect at different concentrations, serial dilutions of the CuS-PEG-c(RGDfK) nanoparticles were
45
46
47
48
49
50
51
52
53
54
55
56
57
58
59
60

irradiated with NIR laser at 3 W/cm^2 . As shown in **Figure 2b**, the temperature increased linearly with the concentration of the nanoparticles. The temperature was elevated to 94.3°C at a nanoparticle concentration of 1 mM . Furthermore, the photothermal effect of CuS-PEG-c(RGDfK) nanoparticles was dependent on the laser power. The temperature increased linearly with the increasing laser power from 0.5 to 2 W/cm^2 (**Figure 2c**).

Figure 2

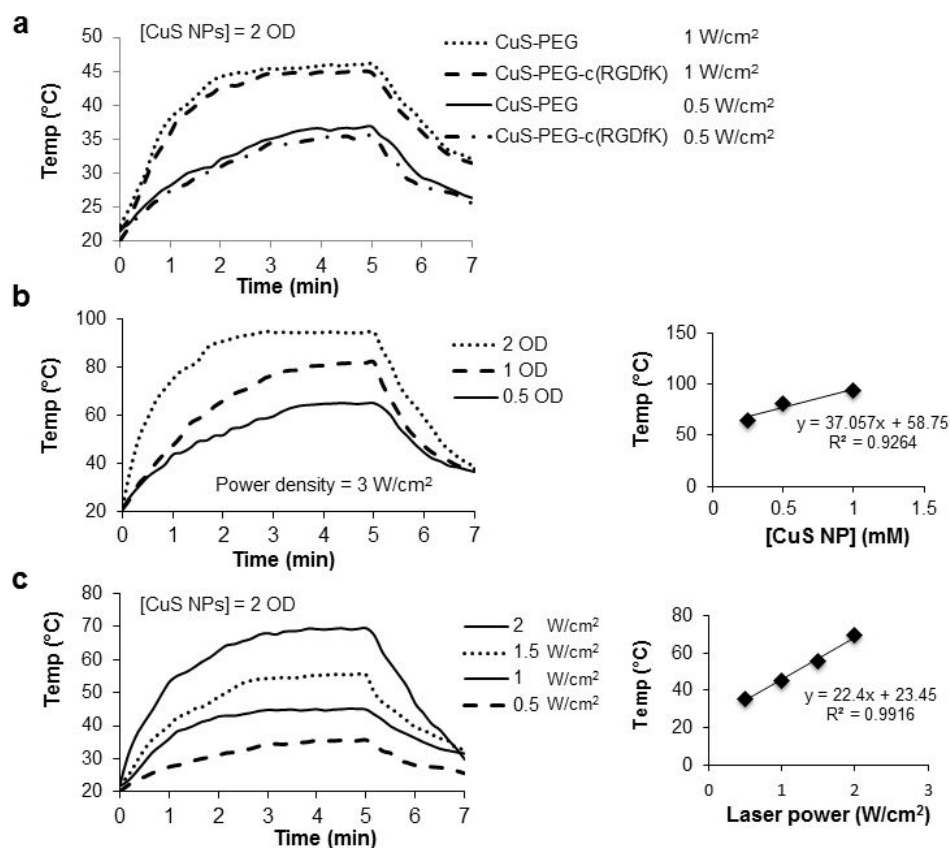


Figure 2. CuS-PEG-c(RGDfK) nanoparticles mediated efficient photothermal effects. (a) Comparison of the photothermal effects of CuS-PEG and CuS-PEG-c(RGDfK) nanoparticles in aqueous solution. **(b)** Photothermal effects of CuS-PEG-c(RGDfK) at different concentrations. **(c)** Photothermal effects of CuS-PEG-c(RGDfK) nanoparticles with different levels of laser power.

1
2
3
4
5
6 **Cytotoxicity study.** The effect of the nanoparticles on cell viability was evaluated by MTS
7
8 assay. In HEK 293 cells, the effects of CuS-PEG nanoparticles, CuS-c(RGDfK) nanoparticles, and
9
10 gold nanorods on cell viability did not differ significantly (**Figure S6a**); cell viability was around
11
12 100% at lower nanoparticle concentrations and decreased to ~70% at the highest concentration (3
13
14 OD, 1.5 mM). In HepG2 cells, no significant difference was observed at the lower nanoparticle
15
16 concentrations, whereas CuS-PEG nanoparticles lowered cell viability at Cu concentrations 0.5
17
18 mM and higher (**Figure S6b**). In U87 cells, the viability was around 100% after treatment with all
19
20 concentrations of CuS-PEG nanoparticles, CuS-c(RGDfK) nanoparticles, or gold nanorods
21
22 (**Figure S6c**). In all three cell lines, the cell viability was significantly lower than in the other
23
24 groups after treatment with cetyltrimethylammonium bromide (CTAB)-stabilized gold
25
26 nanoparticles starting from 0.005 mM.
27
28
29

30
31 **Radiolabeling efficiency and stability.** The radiolabeling efficiency and stability of
32
33 [⁶⁴Cu]CuS-PEG-c(RGDfK) nanoparticles is shown in **Figure S7**. The radiochemical yield was
34
35 >98%. After suspension in phosphate-buffered saline solution (PBS) or human plasma at room
36
37 temperature for 24 h, CuS-c(RGDfK) nanoparticles lost ~0.6% and ~1.7 % of their radioactivity,
38
39 respectively. [⁶⁴Cu]CuS-c(RGDfK) nanoparticles lost about 2.7% and 3.3% radioactivity after 48
40
41 h incubation in PBS or human plasma, respectively.
42
43

44
45 ***In vitro* αvβ3 integrin targeting.** The specific binding of CuS-PEG-c(RGDfK)
46
47 nanoparticles to αvβ3 integrin was investigated using a sandwich ELISA binding assay.²² **Figure**
48
49 **3a** shows that CuS-PEG nanoparticles had minimal detectable binding to the αvβ3 integrin, while
50
51 the binding to αvβ3 integrin of CuS-c(RGDfK) nanoparticles increased with increasing peptide-
52
53 to-PEG ratio. Furthermore, the binding of CuS-PEG-c(RGDfK) (peptide:PEG = 0.13:1 and higher
54
55
56
57
58
59
60

ratios) was significantly higher than that of CuS-PEG nanoparticles without peptide. To study the binding specificity of the CuS-PEG-c(RGDfK) nanoparticles, large excess amounts of c(RGDfK) peptides (50 μ M, 100 μ L) were pre-incubated with α v β 3 protein, followed by addition of different concentrations (1 to 5 OD at 930 nm) of CuS-PEG-c(RGDfK) nanoparticles (peptide:PEG 0.6:1). Binding of CuS-PEG-c(RGDfK) to α v β 3 was completely blocked at 3 different nanoparticle concentrations tested (1, 2.5 and 5 OD) (Figure 3b), demonstrating the excellent binding specificity to α v β 3 integrin.

Figure 3

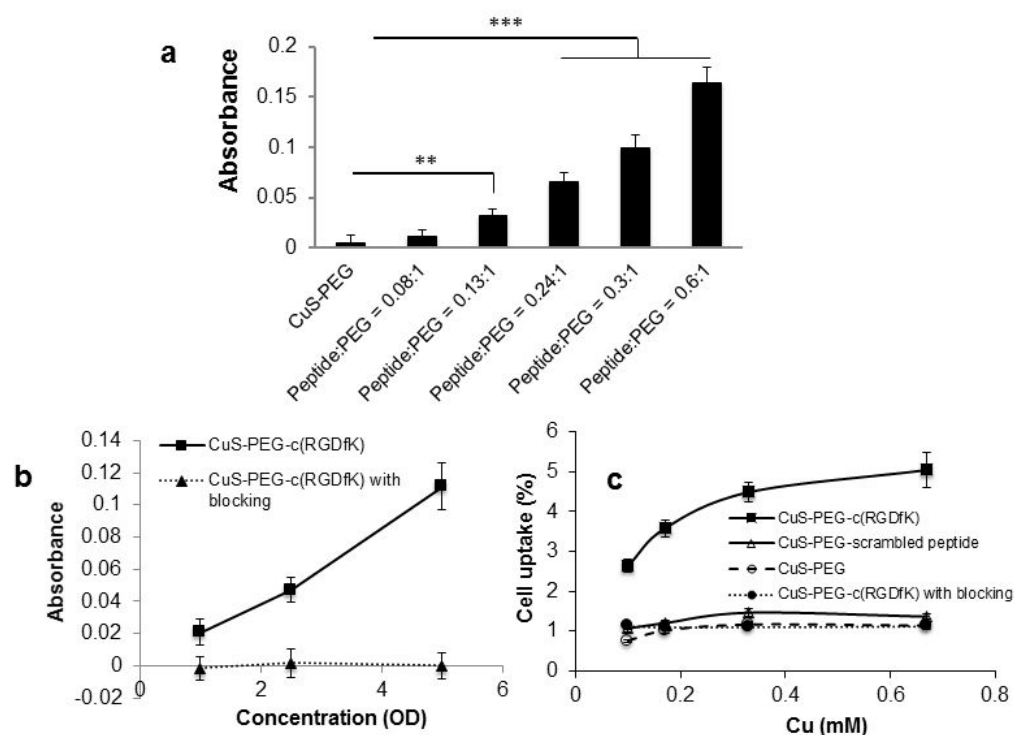


Figure 3. CuS-PEG-c(RGDfK) nanoparticles selectively bound to integrin α v β 3 *in vitro*. (a)

The binding affinity of CuS-PEG-c(RGDfK) nanoparticles at different concentrations on an integrin-coated plate using a sandwich ELISA (n=3); *p<0.05, **p<0.01. (b) Comparison of the

1
2
3 binding affinities of CuS-PEG-c(RGDfK) nanoparticles and CuS-PEG-c(RGDfK) nanoparticles
4 blocked with an excess amount of free c(RGDfK) peptide on an integrin-coated plate using a
5 sandwich ELISA (n=3). (c) Cellular uptake of [⁶⁴Cu]CuS-PEG and [⁶⁴Cu]CuS-PEG-c(RGDfK)
6 nanoparticles in U87 cells (n=6/group).
7
8
9
10
11
12
13
14
15

16 We then evaluated cellular uptake of [⁶⁴Cu]CuS-PEG-c(RGDfK) nanoparticles by U87
17 glioblastoma cells, which express high levels of integrin $\alpha\beta3$ receptors. In this study, [⁶⁴Cu]CuS-
18 PEG-c(RGDfK) nanoparticles exhibited a significant binding to the integrin-overexpressing cells,
19 about three-fold higher than the control nanoparticles, whereas the two controls, [⁶⁴Cu]CuS-PEG
20 and CuS-PEG-scrambled peptide, were taken up by these cells to a similar extent (**Figure 3c**).
21 Moreover, exposure to the free c(RGDfK) peptide blocked this specific binding effect of the
22 [⁶⁴Cu]CuS-PEG-c(RGDfK) nanoparticles, and the cellular uptake was decreased to levels
23 equivalent to those of the control nanoparticles (i.e., CuS-PEG, CuS-PEG-scrambled peptide)
24 (**Figure 3c**). Overall, these results highlighted the high specific affinity of the CuS-PEG-
25 c(RGDfK) nanoparticles to the integrin $\alpha\beta3$ receptors *in vitro*.
26
27
28
29
30
31
32
33
34
35
36
37
38

39 ***In vitro* photothermal ablation.** To demonstrate the targeting effect of the CuS-PEG-
40 c(RGDfK) nanoparticles for photothermal treatment, U87 cells in culture were incubated with
41 CuS-PEG or CuS-PEG-c(RGDfK) nanoparticles at the same concentration (3 OD) for 2 h. After
42 the removal of free nanoparticles, the cells were irradiated with the laser at 3 W/cm² for 2 min. As
43 shown in **Figure 4a**, U87 cells within the laser region were completely depleted after laser
44 treatment via CuS-PEG-c(RGDfK) nanoparticles, while some U87 cells in the irradiated region
45 were still alive for U87 cells exposed to CuS-PEG nanoparticles. For both treatments, the cells in
46 the region outside the laser footprint remained viable. Moreover, this destructive effect was not
47
48
49
50
51
52
53
54
55
56
57
58
59
60

observed in U87 cells treated by NIR laser alone. For quantitative analysis of cell viability, a similar experiment was performed in which U87 cells were treated with CuS-PEG nanoparticles or different concentrations of CuS-PEG-c(RGDfK) nanoparticles. The results (**Figure 4b and c**) reveal that CuS-PEG-c(RGDfK) nanoparticles mediated a more effective photothermal effect against U87 cells. Furthermore, the cell killing effect of CuS-PEG-c(RGDfK) nanoparticles + laser exhibited a concentration-dependent profile. These results indicate that CuS-PEG-c(RGDfK), with their higher uptake in U87 cells, led to more effective photothermal destruction tumor cells within the zone of laser irradiation.

Figure 4

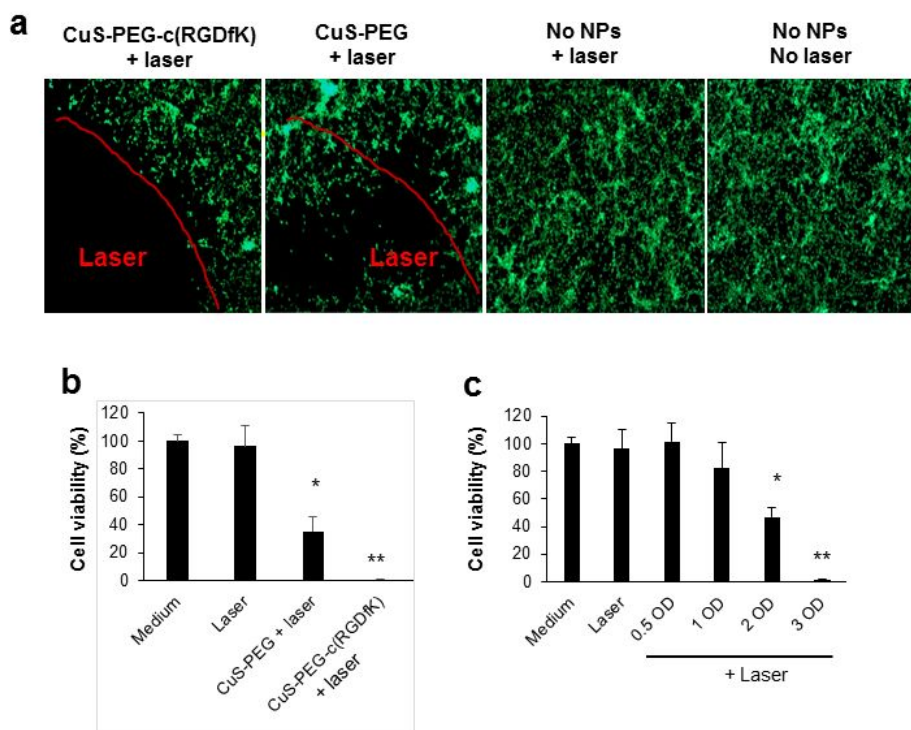


Figure 4. Visualization and quantification of U87 cell ablation after NIR laser treatment *in vitro*. (a) Photothermal ablation of U87 cells using NIR laser mediated by CuS-PEG-c(RGDfK)

1
2
3 or CuS-PEG nanoparticles (NPs). Representative images are shown. Viable U87 cells were stained
4 green. (b) Cell viability after treatment with the same concentration of CuS-PEG-c(RGDfK) or
5 CuS-PEG nanoparticles (1.5 mM) and the same laser power (n=5/group). (c) Cell viability after
6 treatment with different concentrations (0.25-1.5 mM) of CuS-PEG-c(RGDfK) nanoparticles
7 (n=5/group; *p<0.05, **p<0.01 compared to blank control).
8
9
10
11
12
13
14
15
16

17 **μ PET/CT imaging and biodistribution.** *In vivo* PET/CT imaging with [⁶⁴Cu]CuS-PEG-
18 c(RGDfK) or [⁶⁴Cu]CuS-PEG nanoparticles was acquired 24 h after intravenous injection of one
19 of these nanoparticle formulations into U87 tumor-bearing mice. The results revealed significantly
20 higher tumor uptake of [⁶⁴Cu]CuS-PEG-c(RGDfK) nanoparticles than of [⁶⁴Cu]CuS-PEG
21 nanoparticles (**Figure 5a**). On the basis of quantitative region of interest analysis for the
22 representative PET/CT images, the tumor uptake of targeted [⁶⁴Cu]CuS-PEG-c(RGDfK)
23 nanoparticles at 24 h was 10.3%ID/g, whereas the tumor uptake of non-targeted [⁶⁴Cu]CuS-PEG
24 nanoparticles was only 4.9%ID/g. The localization of the [⁶⁴Cu]CuS-PEG-c(RGDfK) and the
25 [⁶⁴Cu]CuS-PEG nanoparticles was determined by a biodistribution study in the same groups of
26 mice (**Figure 5b**). No significant differences in liver, spleen, and kidney uptake were observed
27 between [⁶⁴Cu]CuS-PEG-c(RGDfK) and [⁶⁴Cu]CuS-PEG. The tumor uptake for [⁶⁴Cu]CuS-PEG-
28 c(RGDfK) ($9.44 \pm 1.18\%$ ID/g) was significantly higher than that of [⁶⁴Cu]CuS-PEG ($4.31 \pm$
29 1.36% ID/g) (p<0.05). These results confirmed the observation of higher tumor cell uptake by
30 [⁶⁴Cu]CuS-PEG-c(RGDfK) nanoparticles, suggesting the superb targeting efficiency and
31 specificity of RGD-conjugated CuS nanoparticles in integrin $\alpha v \beta 3$ -overexpressing tumors.
32
33
34
35
36
37
38
39
40
41
42
43
44
45
46
47
48
49
50
51
52
53
54
55
56
57
58
59
60

Figure 5

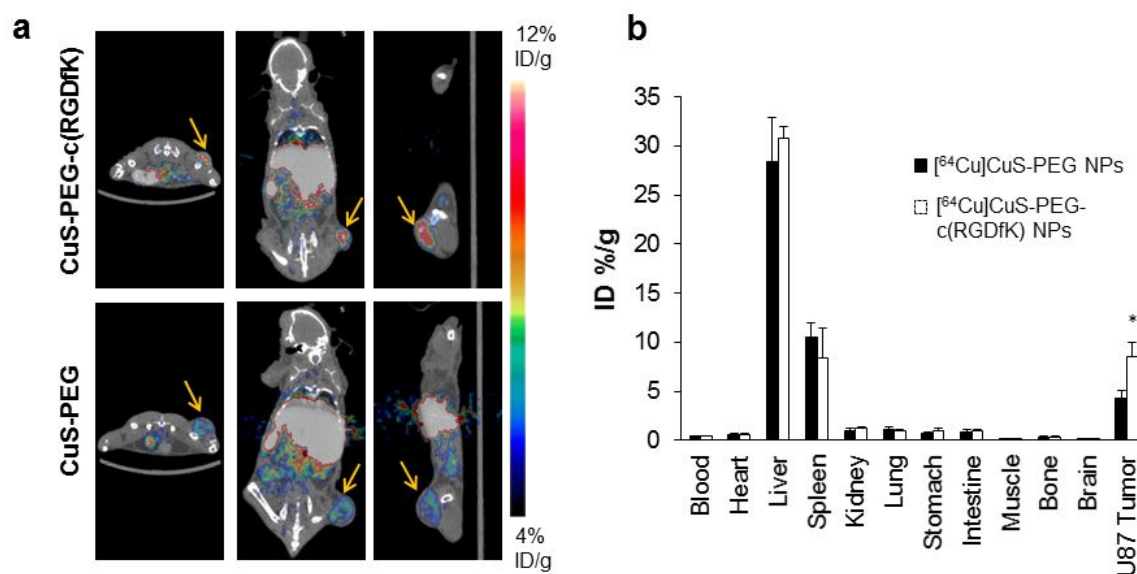
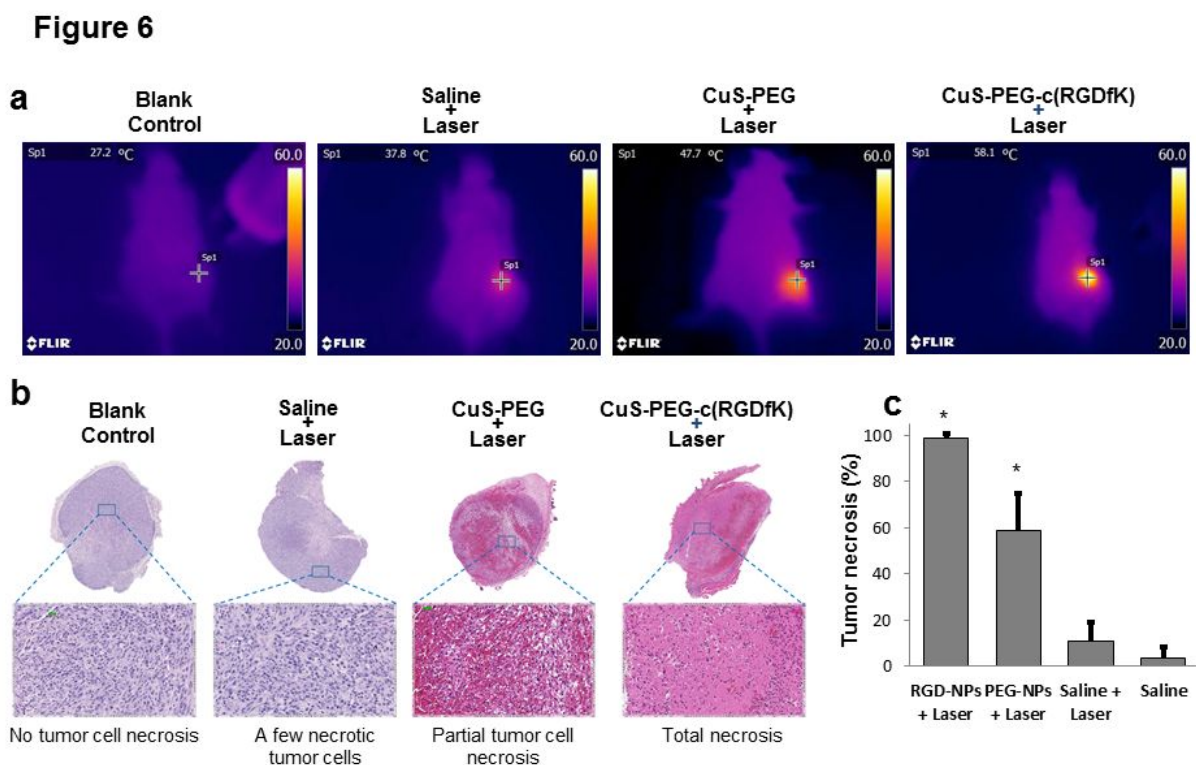


Figure 5. c(RGDfK)-tagged CuS nanoparticles increased the tumor-targeting efficiency over untagged nanoparticles. (a) PET/CT images of representative nude mice bearing a U87 xenograft tumor. Images were acquired 24 h after intravenous injection of $[^{64}\text{Cu}]\text{CuS-PEG-c(RGDfK)}$ or $[^{64}\text{Cu}]\text{CuS-PEG}$ nanoparticles. The arrows point to the tumor. (b) Biodistribution of $[^{64}\text{Cu}]\text{CuS-PEG}$ and $[^{64}\text{Cu}]\text{CuS-PEG-c(RGDfK)}$ nanoparticles (NPs) 24 h after intravenous administration of nanoparticles ($n=4/\text{group}$; $p<0.05$).

***In vivo* photothermal ablation therapy.** The therapeutic effects of CuS-PEG-c(RGDfK) and CuS-PEG were examined with an 808-nm continuous-wave laser in U87 tumor-bearing mice.

The tumor temperature increased from 38°C in the mouse that received saline solution and NIR laser irradiation to 47.7°C in the mouse treated with CuS-PEG nanoparticles and NIR laser, and further increased to 58.1°C in the mouse administered CuS-c(RGDfK) nanoparticles and received NIR laser (**Figure 6a**). Histological analysis of the tumors, removed 24 h after laser treatment, confirmed that the treatment with CuS-PEG-c(RGDfK) nanoparticles and NIR laser led to a greater necrotic response than treatment with CuS-PEG nanoparticles and NIR laser (**Figure 6b and c**); about 98% of tumor tissue was necrotic in the tumors treated with CuS-PEG-c(RGDfK) nanoparticles, whereas the fraction of necrotized tissue was ~60% in the tumors treated with CuS-PEG nanoparticles and laser. For the tumors treated with saline solution and laser, the fraction of necrosis was at the baseline level of <5%.



1
2
3 **Figure 6. c(RGDfK)-tagged CuS nanoparticles mediated effective photothermal ablation of tumors in U87**
4 **xenograft-bearing mice. (a)** Temperature at the tumor site during photothermal ablation study. **(b)** Representative
5 microphotographs of histologic sections of tumors removed 24 h after photothermal ablation. **(c)** Quantitative analysis
6 of the percentage of necrosis induced by different treatments; NPs, nanoparticles. NIR laser treatment was instituted
7 for 3 min at a power density of 4 W/cm².**Discussion**

12
13 Attaching targeting ligands to the surface of nanoparticles for targeting nanoparticle
14 delivery to solid tumor have been attempted in numerous preclinical studies, with limited
15 success.²³ Targeting surface receptors expressed in both angiogenic blood vessel and tumor cells
16 is attractive because even if binding of nanoparticles to tumor cells may be impeded by limited
17 extravasation into the extravascular fluid space and inefficient convection towards tumor cells,
18 selective binding to tumor vasculature should still be possible. In this study, we report robust
19 conjugation of cyclic c(RGDfK) peptide to PEG-coated CuS nanoparticles using click chemistry,
20 and successful demonstration of selective binding of c(RGDfK)-tagged CuS nanoparticles to $\alpha\beta3$
21 integrin both *in vitro* and *in vivo*.

22
23
24
25
26
27
28
29
30
31
32
33
34 Conjugation of c(RGDfK) to the terminus of PEG coating on the surface of CuS
35 nanoparticles did not affect their optical and photothermal conversion properties. *In vitro* binding
36 to $\alpha\beta3$, evaluated using a modified ELISA assay, showed an increased binding of CuS-PEG-
37 c(RGDfK) nanoparticles to $\alpha\beta3$ -coated plates with increasing peptide density on the surface of
38 nanoparticles. Such binding could be completely blocked by free c(RGDfK). In addition, cellular
39 uptake of CuS-PEG-c(RGDfK) nanoparticles in $\alpha\beta3$ -expressing U87 cells increased with
40 increasing nanoparticle concentration, which again, could be completely blocked by free
41 c(RGDfK). These data, together with the finding that CuS-PEG-scrambled peptide did not bind to
42 $\alpha\beta3$ integrin, indicate that c(RGDfK)-tagged CuS nanoparticles selectively bind to $\alpha\beta3$ receptor.

1
2
3 *In vitro* cytotoxicity studies revealed that CuS-PEG-c(RGDfK) nanoparticles and gold
4 nanoparticles, which are thought to be biocompatible, exhibited similar cytotoxicities in all three
5 cell lines tested. The viability of HepG2 and U87 cells treated with either of these nanoparticles
6 was ~100% at all the concentrations tested, from 0.00015 to 1.5 mM, while the viability of HEK
7 293 cells was decreased slightly, to ~80%, at higher nanoparticle concentrations. In contrast,
8 CTAB-stabilized gold nanorods that are commonly used in photothermal ablation applications
9 exhibited significant cytotoxicity in all three cell lines.

19 To facilitate quantitative analysis of the biodistribution of nanoparticles *in vivo*, we labeled
20 both CuS-PEG and CuS-PEG-c(RGDfK) nanoparticles with the positron emitter ^{64}Cu without the
21 use of any radiometal chelator as ^{64}Cu was efficiently incorporated into the matrix of CuS
22 nanoparticles. $\mu\text{PET/CT}$ imaging was applied to assess the *in vivo* biodistribution of the CuS-PEG-
23 c(RGDfK) nanoparticles. Almost all the ^{64}Cu (>98%) was successfully integrated into the CuS
24 nanoparticles at the end of the synthesis. ^{64}Cu -labeled nanoparticles displayed high labeling
25 stability: the ^{64}Cu nanoparticles lost only ~3% of radioactivity after
26 incubation in PBS or human plasma at room temperature for 48 h. The $\mu\text{PET/CT}$ and
27 biodistribution studies showed that both ^{64}Cu nanoparticles were almost completely cleared from blood circulation 24 h after injection.
28 ^{64}Cu nanoparticles were almost completely cleared from blood circulation 24 h after injection.
29 ^{64}Cu nanoparticles were almost completely cleared from blood circulation 24 h after injection.
30 ^{64}Cu nanoparticles were almost completely cleared from blood circulation 24 h after injection.
31 ^{64}Cu nanoparticles were almost completely cleared from blood circulation 24 h after injection.
32 ^{64}Cu nanoparticles were almost completely cleared from blood circulation 24 h after injection.
33 ^{64}Cu nanoparticles were almost completely cleared from blood circulation 24 h after injection.
34 ^{64}Cu nanoparticles were almost completely cleared from blood circulation 24 h after injection.
35 ^{64}Cu nanoparticles were almost completely cleared from blood circulation 24 h after injection.
36 ^{64}Cu nanoparticles were almost completely cleared from blood circulation 24 h after injection.
37 ^{64}Cu nanoparticles were almost completely cleared from blood circulation 24 h after injection.
38 ^{64}Cu nanoparticles were almost completely cleared from blood circulation 24 h after injection.
39 ^{64}Cu nanoparticles were almost completely cleared from blood circulation 24 h after injection.
40 ^{64}Cu nanoparticles were almost completely cleared from blood circulation 24 h after injection.
41 ^{64}Cu nanoparticles were almost completely cleared from blood circulation 24 h after injection.
42 ^{64}Cu nanoparticles were almost completely cleared from blood circulation 24 h after injection.
43 ^{64}Cu nanoparticles were almost completely cleared from blood circulation 24 h after injection.
44 ^{64}Cu nanoparticles were almost completely cleared from blood circulation 24 h after injection.
45 ^{64}Cu nanoparticles were almost completely cleared from blood circulation 24 h after injection.
46 ^{64}Cu nanoparticles were almost completely cleared from blood circulation 24 h after injection.
47 ^{64}Cu nanoparticles were almost completely cleared from blood circulation 24 h after injection.
48 ^{64}Cu nanoparticles were almost completely cleared from blood circulation 24 h after injection.
49 ^{64}Cu nanoparticles were almost completely cleared from blood circulation 24 h after injection.
50 ^{64}Cu nanoparticles were almost completely cleared from blood circulation 24 h after injection.
51 ^{64}Cu nanoparticles were almost completely cleared from blood circulation 24 h after injection.
52 ^{64}Cu nanoparticles were almost completely cleared from blood circulation 24 h after injection.
53 ^{64}Cu nanoparticles were almost completely cleared from blood circulation 24 h after injection.
54 ^{64}Cu nanoparticles were almost completely cleared from blood circulation 24 h after injection.
55 ^{64}Cu nanoparticles were almost completely cleared from blood circulation 24 h after injection.
56 ^{64}Cu nanoparticles were almost completely cleared from blood circulation 24 h after injection.
57 ^{64}Cu nanoparticles were almost completely cleared from blood circulation 24 h after injection.
58 ^{64}Cu nanoparticles were almost completely cleared from blood circulation 24 h after injection.
59 ^{64}Cu nanoparticles were almost completely cleared from blood circulation 24 h after injection.
60 ^{64}Cu nanoparticles were almost completely cleared from blood circulation 24 h after injection.

1
2
3 the spleen is to make CuS nanodots with average size of less than 6 nm, as have been shown recently.³
4
5 These ultrasmall CuS nanodots were cleared via the renal-urinary system and exhibited low uptake
6
7 in the liver and the spleen.
8
9

10 Higher uptake of CuS-PEG-c(RGDfK) nanoparticles in tumor cells than CuS-PEG
11 nanoparticles led to more efficient photothermal killing of U87 tumor cells *in vitro* with $\alpha\beta3$ -
12 targeting CuS nanoparticles. Higher tumor deposition of CuS-PEG-c(RGDfK) than CuS-PEG *in*
13 *vivo* resulted in more than 10°C higher temperature elevation of laser-irradiated tumors under the
14 same laser treatment conditions: a tumor temperature of 47.7°C was achieved with CuS-PEG
15 nanoparticles and NIR laser, whereas a much higher temperature of 58.1°C was achieved with
16 CuS-PEG-c(RGDfK) nanoparticles and NIR laser instituted for 3 min at a power density of 4
17 W/cm². Under the laser treatment conditions used, almost the entire tumor became necrotic with
18 CuS-PEG-c(RGDfK), whereas only partial tumor ablation was achieved with the CuS-PEG
19 nanoparticles. These data indicate that successful targeting of CuS-PEG-c(RGDfK) nanoparticles
20 to tumor vasculature and $\alpha\beta3$ integrin-expressing tumor cells mediated efficient photothermal
21 ablation of tumors *in vivo*.
22
23
24
25
26
27
28
29
30
31
32
33
34
35
36
37
38
39

40 CONCLUSIONS

41
42 We have developed a robust procedure for the introduction of targeting ligand to the surface
43 of CuS and [⁶⁴Cu]CuS nanoparticles via PEG linkers using click chemistry. [⁶⁴Cu]CuS-PEG-
44 c(RGDfK) demonstrated selective uptake in U87 tumors. PTA ablation of U87 tumors was also
45 significantly more efficient with CuS-PEG-c(RGDfK) nanoparticles than with non-targeted CuS-
46 PEG nanoparticles. These results indicate that [⁶⁴Cu]CuS-PEG-c(RGDfK) can be used not only
47
48
49
50
51
52
53
54
55
56
57
58
59
60

1
2
3 for molecular imaging of angiogenic blood vessels, but also for PET/CT image-guided PTA
4
5 therapy.
6
7
8
9
10

11 12 **MATERIALS AND METHODS** 13

14 **Materials.** 1-Ethyl-3-[3-dimethylaminopropyl]carbodiimide hydrochloride (EDAC), 4-
15 (2-hydroxyethyl)-1-piperazineethanesulfonic acid (HEPES), 4-pentynoic acid, acetonitrile,
16
17 ammonia hydroxide, benzotriazol-1-yl-oxytripyrrolidinophosphonium hexafluorophosphate (Py-
18
19 BOP), bovine serum albumin (BSA), calcein AM, copper chloride, copper sulfate pentahydrate,
20
21 DMEM cell culture medium, DMEM cell culture medium without phenol red, dimethyl sulfoxide
22
23 (DMSO), ethylenediaminetetraacetic acid (EDTA), ethyl 4-bromobutyrate, ethyl ether, fetal
24
25 bovine serum (FBS), hydrochloric acid (HCl), hydroxybenzotriazole (HOBt), hydrazine,
26
27 methylene chloride (DCM), N,N-diisopropylethylamine (DIPCDI), 1,3 diisopropylcarbodiimide
28
29 (DIPCDI), N-hydroxyl succinimide (NHS), PBS, PBS without Mg and Ca, 0.9% saline solution
30
31 (sodium chloride injection), sodium azide, sodium chloride, sodium ascorbate, sodium hydroxide,
32
33 sodium sulfate, sodium sulfide nonahydrate, trypsin-EDTA solution 0.25%, triethylsilane (TES),
34
35 and trifluoroacetic acid (TFA) were purchased from Sigma-Aldrich (St. Louis, MO). Avidin-
36
37 horseradish peroxidase (HRP), dimethylformamide (DMF), methanol, and piperidine were
38
39 purchased from Fisher Scientific (Hampton, NH). The biotin-anti-PEG conjugation kit was
40
41 purchased from Abcam (Cambridge, UK). Fmoc-Arg(Pbf)-OH, Fmoc-Asp(Wang resin LL)-
42
43 ODmab, Fmoc-Gly-OH, Fmoc-Lys(Mtt)-OH, and Fmoc-Phe-OH were purchased from
44
45 Novabiochem (Billerica, MA). Thiol-PEG-amine (MW 5000 Da) was purchased from Nanocs Inc.
46
47 (New York, NY). $^{64}\text{CuCl}_2$ was produced by the cyclotron research facility at The University of
48
49
50
51
52
53
54
55
56
57
58
59
60

1
2
3 Texas MD Anderson Cancer Center (Houston, TX). Tetramethylbenzidine (TMB) ELISA
4 substrate solution and stop solution were purchased from Life Technologies (Carlsbad, CA). Wash
5
6 buffer (1× PBS with 0.05% Tween 20) was purchased from AbD Serotec (Kidlington, UK).
7
8
9
10 Integrin $\alpha\text{v}\beta\text{3}$ protein was purchased from Chemicon International (Temecula, CA).

11
12 **Synthesis of thiol-PEG-azide.** Azide-modified PEG was synthesized as previously
13 described in the literature.²⁴ Briefly, the starting reactants ethyl 4-bromobutyrate (5.85 g, 30 mmol)
14 and sodium azide (2.925 g, 45 mmol) were added into DMSO (20 mL) with stirring. The reaction
15 mixture was stirred for 22 h at 55°C and cooled to room temperature. Water was added to the
16 reaction mixture and then extracted three times, each with 30 mL of ethyl ether. The combined
17 organic layer was washed with water and brine, and a rotary evaporator was used to remove the
18 organic solvent to yield 3.67 g of ethyl 4-azidobutyrate. Ethyl 4-azidobutyrate (3.14 g, 20 mmol)
19 was dissolved in sodium hydroxide aqueous solution (1 N, 24 mL) with a minimum amount of
20 methanol to make the solution homogeneous. The reaction mixture was stirred for 3 h at room
21 temperature. Methanol was removed using a rotary evaporator and then the aqueous solution was
22 acidified to pH 0 with HCl. After extraction with 50 mL ethyl ether three times, the ether layer
23 was dried with an excess amount of sodium sulfate and filtered. The ethyl ether was then removed
24 with a rotary evaporator to afford 2.11 g of 4-azidobutyric acid. N-hydroxyl succinimide (1.65 g,
25 14.3 mmol) was added into methylene chloride (100 mL), followed by 4-azidobutyric acid (1.68
26 g, 13 mmol) and EDAC (2.74 g, 14.3 mmol). After stirring for 4 h at room temperature, the reaction
27 mixture was washed with water and brine, dried with an excess amount of sodium sulfate, and
28 filtered. The organic solvent was then removed with a rotary evaporator to yield 0.61 g of
29 succinimidyl 4-azidobutyrate. Succinimidyl 4-azidobutyrate was reacted with thiol-PEG-amine in
30 0.1 M HEPES with 0.15 M NaCl pH 8.0 for 2 h at a 2:1 molar ratio. The final product was purified
31
32
33
34
35
36
37
38
39
40
41
42
43
44
45
46
47
48
49
50
51
52
53
54
55
56
57
58
59
60

1
2
3 by dialysis with a filtration membrane with molecular cut-off of 5,000 Da. Thiol-PEG-azide (SH-
4 PEG-N₃) was collected after lyophilization.
5
6

7
8 **Synthesis of alkyne-modified c(RGDfK) peptide.** Alkyne-modified cyclic Arg-Gly-Asp-
9 Phe-Lys peptide was synthesized using Fmoc solid-phase strategy as described in the literature.¹⁸
10 Amino acids (3 eq) were coupled stepwise on the resin in the presence of DIPCDI (3 eq) and HOBt
11 (3 eq) as coupling reagents. After removal of the Dmab- and Fmoc-protecting groups using 2%
12 hydrazine (3 eq) in DMF and 20% piperidine in DMF, respectively, head and tail cyclization on
13 the resin was carried out in DMF using Py-BOP (3 eq), HOBt (3 eq), and DIPCDI (6 eq) as
14 coupling agents. After cyclization, Mtt-protecting group was selectively removed by treatment
15 with TFA/TES/DCM (1/2/97) to yield cyclo- [Lys-Arg(Pbf)-Gly-Asp(resin)-phe]. Then 4-
16 pentynoic acid (3 eq) and DIPCDI (6 eq) were added in DCM for 30 min, followed by addition of
17 HOBt (6 eq). After stirring for 2 h at room temperature, the resin with cyclo- [Lys-Arg(Pbf)-Gly-
18 Asp(resin)-phe]. peptides was added into the 4-pentynoic/DIPCDI/HOBt reaction mixture. After
19 mixing overnight at room temperature, the resin was washed with 5 mL of DMF and DCM three
20 times. Final deprotection and cleavage of the peptides from the resin were simultaneously achieved
21 by treatment with TFA/H₂O/TES (95/1/4, v/v/v) to yield alkyne-modified c(RGDfK) peptide. The
22 product was purified by high-performance liquid chromatography, using the following eluting
23 conditions: solvent: A, 0.1% TFA in water; B, 0.1% TFA in acetonitrile; gradient: B, 0-10% over
24 0-10 min; B, 10-50% over 10-12 min; B, 50-80% over 12-20 min; B, 80% to 10% over 20-21 min.
25 The flow rate was 1 mL/min. The final product was validated using LC/MS time-of-flight mass
26 spectrometer equipped with a Vydac C-18 column (4.6×250.0 mm, 7-μm particle size, 300-Å pore
27 size).
28
29
30
31
32
33
34
35
36
37
38
39
40
41
42
43
44
45
46
47
48
49
50
51
52
53
54
55
56
57
58
59
60

1
2
3 **Synthesis of N₃-PEG-CuS nanoparticles.** The procedure for the synthesis of N₃-PEG-
4 CuS nanoparticles in water was similar to a general procedure reported previously.⁵ In brief, 20
5 mL of aqueous CuCl₂ (1 mM) solution was added to 1 mg of thiol-PEG-N₃ and stirred for 5 min.
6
7 Then, 20 μL of sodium sulfide solution (Na₂S, 1 M) was added to the reaction mixture with stirring
8 at room temperature. The mixture solution turned dark-brown immediately once sodium sulfide
9 was added. After stirring for 5 min, the mixture was heated to 90°C and stirred for another 15 min
10 until the color changed to dark green. The mixture was cooled in an ice-water bath.
11
12
13
14
15
16
17
18

19 **Synthesis of CuS-PEG-c(RGDfK) nanoparticles.** N₃-PEG-CuS nanoparticles (20 mL)
20 were reacted with alkyne-modified c(RGDfK) peptide (PEG:peptide ratio 1:1) at 90°C in the
21 presence of copper sulfate and sodium ascorbate (0.05 eq and 0.1 eq, respectively) as the catalysts.
22
23 The reaction mixture was stirred for 2 h, then purified through a dialysis membrane with MW CO
24 6,000-8,000. The overall synthesis scheme for targeted CuS nanoparticles is shown in **Figure 1**.
25
26
27
28
29
30

31 **Characterization of CuS-PEG-c(RGDfK) nanoparticles.** UV-vis spectra of CuS-PEG
32 and CuS-PEG-c(RGDfK) nanoparticles were examined with a UV-vis DU-800 spectrometer
33 (Beckman-Coulter, Brea, CA) with a 1.0-cm optical path length quartz cuvette. Under aqueous
34 conditions, the particle size, size distribution, and surface charge were investigated by dynamic
35 light scattering (DLS) (Brookhaven Instruments Corporation, Holtsville, NY). Transmission
36 electron microscopy (TEM) images were acquired using a transmission electron microscope (JEM
37 2010, JEOL Japan) at an accelerating voltage of 200 kV. Aqueous solution of CuS NPs was
38 deposited on carbon-enhanced copper grids without negative staining. Amino acid analysis was
39 used to quantify the amount of peptide attached to the surface of the nanoparticles. For sample
40 preparation, the nanoparticles were dissolved in ammonia hydroxide and then dried in a hydrolysis
41
42
43
44
45
46
47
48
49
50
51
52
53
54
55
56
57
58
59
60

1
2
3 tube. Hydrochloric acid (6 N) was added to the tube. After the peptide was hydrolyzed at 110°C
4
5 for 24 h, the mixture was dried and dissolved in water for amino acid analysis.
6

7
8 **Sandwich ELISA binding study.** Ninety-six-well plates were coated with purified $\alpha\beta 3$
9
10 integrin protein at 0.1 $\mu\text{g}/\text{well}$ and kept at 4°C overnight. The plates were washed in a washing
11
12 buffer (1× PBS with 0.05% Tween 20) after incubation and then blocked with blocking buffer (1×
13
14 PBS with 2% BSA) at room temperature for 2 h. The blocking buffer was removed, and the plates
15
16 were inoculated in triplicate with CuS-PEG (control) or CuS-PEG-c(RGDfK) at a series of
17
18 PEG:c(RGDfK) peptide ratios. A solution of nanoparticles (1 OD) was prepared using blocking
19
20 buffer containing Ca^{2+} and Mg^{2+} and then incubated at room temperature for 1 h. The detection
21
22 antibody biotin-anti-PEG, which recognizes the backbone of the PEG molecule, was added at 0.05
23
24 $\mu\text{g}/\text{well}$. The plates were incubated at room temperature for 1 h, then washed, and the bound biotin-
25
26 anti-PEG was detected using avidin-HRP conjugate at 0.005 $\mu\text{g}/\text{well}$. After washing, 100 μL of
27
28 substrate solution was added to each well and the luminescence was read. The resulting
29
30 luminescence signal intensity was plotted against PEG:c(RGDfK) peptide ratios. To validate the
31
32 binding specificity, a blocking study was performed with incubation of excess c(RGDfK) peptide
33
34 similar to the ELISA binding study. The concentration of c(RGDfK) was 50 μM (100 $\mu\text{L}/\text{well}$).
35
36
37
38
39

40 **Cell culture.** Human hepatocellular carcinoma cells (HepG2), human kidney epithelial
41
42 cells (HEK 293), and human glioblastoma cells (U87) were purchased from ATCC (Manassas,
43
44 VA) and were cultured in Eagle minimum essential medium. The cell lines were maintained at
45
46 37°C in a humidified atmosphere containing 5% CO_2 . The U87 cells expressed high levels of $\alpha\beta 3$
47
48 integrin on the surface of cells.¹⁶ HepG2 and HEK 293 cells were used as models for testing the
49
50 cytotoxicity of the nanoparticles for liver and kidney cells, respectively. Citrate-stabilized gold
51
52 nanoparticles and CTAB-stabilized gold nanorods were used as controls.
53
54
55
56
57
58
59
60

1
2
3 **Cytotoxicity study.** HepG2, HEK 293, and U87 cells were seeded separately at a density
4 of 1×10^4 cells/well in a 96-well plate and incubated for at least 24 h prior to treatment. The cells
5 were treated with culture medium alone, or gold NPs, gold nanorods, PEG-CuS nanoparticles, and
6 c(RGDfK)-CuS nanoparticles in culture media, respectively, at different concentrations (1.5, 0.5,
7 0.15, 0.05, 0.015, 0.005, 0.0015, 0.0005 and 0.00015 mM equivalent [Cu] or [Au]) for 24 h in an
8 incubator at 37°C in an atmosphere containing 5% CO₂. MTS working solution was then pipetted
9 into each well and the cells were incubated at 37°C for an additional 3 h. The absorption was
10 measured at 490 nm using an ELx800 microplate reader (BioTek Instruments, Winooski, VT).
11 Each sample was prepared in sextuplet, and the data are reported as means \pm standard deviation.
12
13
14
15
16
17
18
19
20
21
22
23

24 **Cellular uptake studies.** U87 cells were seeded in a 24-well plate at a density of
25 6×10^4 /well and were incubated for at least 24 h before treatment. [⁶⁴Cu]CuS-PEG or [⁶⁴Cu]CuS-
26 PEG-c(RGDfK) nanoparticles at different concentrations (0.1, 0.17, 0.33 and 0.67 mM equivalent
27 [Cu]) were added to the wells and incubated at 37°C for 2 h. For the blocking assay, the cells were
28 incubated with a large excess of c(RGDfK) peptide (500 μM) for 2 h, followed by addition of
29 [⁶⁴Cu]CuS-PEG-c(RGDfK) nanoparticles at different concentrations. The mixture was incubated
30 at 37°C for 2 h. The cells were then washed three times with PBS and collected after treatment
31 with 200 μL of trypsin. The cell-associated radioactivity was measured with a Packard Cobra
32 gamma counter (GMI Inc, Ramsey, MN). Each sample was prepared in sextuplet, and the data are
33 reported as means \pm standard deviation.
34
35
36
37
38
39
40
41
42
43
44
45
46

47 **Photothermal effect in aqueous solution.** To compare the photothermal effects of the
48 CuS-PEG and CuS-PEG-c(RGDfK) nanoparticles, a 15PLUS laser (Diomed, Andover, MA) with
49 a continuous-wave, center wavelength of 808 ± 10 nm, was used. To transfer the laser power from
50 the laser unit to the aqueous solution of nanoparticles, a 5 m, core LCM-001 optical fiber (BioTex
51
52
53
54
55
56
57
58
59
60

1
2
3 Inc., Houston, TX) was attached to a retort stand via a clamp. The end of the fiber was placed
4 directly above the tube containing the aqueous solution. The temperature changes mediated by
5 nanoparticles under NIR laser light were measured through an i7 thermal camera (Flir Systems
6 Inc., Portland, OR). Water was used as the control.
7
8
9
10
11

12 ***In vitro* photothermal ablation study.** U87 cells were seeded onto a 24-well plate at a
13 density of 6×10^4 per well and were incubated for at least 24 h prior to treatment. Cells were washed
14 three times with PBS and then incubated with CuS-PEG nanoparticles or CuS-PEG-c(RGDfK)
15 nanoparticles (1.5 mM of [Cu]), n=3) in DMEM at 37°C for 2 h. Cells not incubated with
16 nanoparticles and not laser irradiated were used as negative controls. After treatment with
17 nanoparticles, the culture medium was replaced with fresh DMEM without phenol red, and the
18 cells were irradiated with a diode NIR laser centered at 808 nm at an output power of 3 W/cm² for
19 2 min. After the treatment, cells were re-supplied with DMEM containing 10% FBS. After 24 h,
20 the cells were washed with PBS and stained with 1 μM calcein AM solution (5 μL calcein AM
21 stock solution added to 10 mL of PBS); viable cells were visualized under a Zeiss Axio
22 Observer.Z1 fluorescence microscope. To quantify the dead cells after photothermal ablation, U87
23 cells were treated with nanoparticles and NIR laser irradiation as just described. After the cells
24 were washed with PBS, MTS working solution was added to the cells, and the absorption was
25 measured 3 h later at 490 nm using a microplate reader. The data were reported as means ± standard
26 deviation.
27
28
29
30
31
32
33
34
35
36
37
38
39
40
41
42
43
44
45
46

47 **Radiolabeling of CuS-PEG-c(RGDfK) nanoparticles.** ⁶⁴CuCl₂ (20 μL, 1000 μCi) was
48 added to 20 mL of CuCl₂ solution (1 mM), followed by 1 mg thiol-PEG-N₃. After addition of 2
49 μL of sodium sulfide solution (1 M) into the dark CuCl₂ solution, the mixture was heated to 90°C
50 for 15 min until the color of the solution turned green. The reaction mixture was transferred to ice-
51
52
53
54
55
56
57
58
59
60

1
2
3 cold water to obtain [^{64}Cu]CuS-PEG- N_3 nanoparticles. Then alkyne-modified c(RGDfK) peptide
4 in water (1:1 molar ratio) was added into an aqueous solution of [^{64}Cu]CuS-PEG- N_3 nanoparticles
5
6
7
8 with copper sulfate (0.05 eq.) and sodium ascorbate (0.1 eq.) to catalyze the reaction. The reaction
9
10 mixture was stirred at 90°C for 2 h and was purified using a disposable PD 10 column.

11
12 The radiolabeling efficiency and stability of labeled nanoparticles were analyzed using
13 instant thin-layer chromatography (ITLC). The ITLC strips were developed with PBS (pH 7.4)
14 containing 4 mM EDTA and radioactivity quantified using an IAR-2000 TLC imaging scanner
15
16
17 (Eckert & Ziegler Radiopharma, Berlin, Germany). To study the labeling stability, [^{64}Cu]CuS-
18
19 PEG-c(RGDfK) nanoparticles were suspended in PBS or human plasma and incubated at room
20
21
22 temperature for 24 h or 48 h. Free $^{64}\text{Cu}^{2+}$ ions moved to the top of the ITLC strip, while the
23
24
25 nanoparticles remained at the original spot. The radioactivity at the original spot was recorded as
26
27
28 a percentage of the total radioactivity applied to the ITLC strip.

29
30
31 **$\mu\text{PET}/\text{CT}$ imaging and biodistribution.** All animal studies followed protocols and
32 guidelines approved by the Institutional Animal Care and Use Committee at The University of
33
34
35 Texas MD Anderson Cancer Center. Eight- to 10-week-old female nude mice (Harlan-Sprague-
36
37
38 Dawley, Indianapolis, IN) were inoculated subcutaneously with human U87 glioblastoma cells
39
40
41 (7×10^6 cells/mouse) in the right thigh. When tumors had grown to 5-8 mm in diameter, mice were
42
43
44 randomly allocated into two groups ($n=3/\text{group}$). Mice in Group A received an intravenous
45
46
47 injection of [^{64}Cu]CuS-PEG-c(RGDfK) nanoparticles (200 $\mu\text{Ci}/\text{mouse}$; 0.2 mL). Mice in Group B
48
49
50 received an intravenous injection of [^{64}Cu]CuS-PEG nanoparticles (200 $\mu\text{Ci}/\text{mouse}$; 0.2 mL).
51
52
53 Twenty-four hours after injection of the radiolabeled nanoparticles, the animals were anesthetized
54
55
56 with a mixture of isoflurane and oxygen gas (2% of isoflurane) and placed in a prone position, and
57
58
59 images were acquired using an Inveon $\mu\text{PET}/\text{CT}$ scanner (Siemens Medical Solutions, Erlangen,
60

Germany). The μ PET and CT images were generated separately and then fused using Inveon Research Workplace software. After μ PET/CT imaging, the mice were euthanized by CO₂ inhalation, and their blood, heart, liver, spleen, kidneys, lungs, stomach, intestine, muscle, bone, brain, and tumor tissues were harvested and weighed; the radioactivity of each tissue was measured with a Packard Cobra gamma counter (GMI, Inc., Ramsey, MN). Uptake of ⁶⁴Cu-labeled CuS nanoparticles in various organs was expressed as percentage of injected dose per gram of tissue (%ID/g). The data were expressed as means \pm standard deviation.

In vivo photothermal ablation therapy. When the tumors had grown to 7-10 mm in diameter, mice were randomly allocated into four groups (n=4 each). Mice in group A were injected intravenously with CuS-PEG-c(RGDfK) nanoparticles (200 μ L, 4 mM/mouse). Mice in group B were injected intravenously with CuS-PEG nanoparticles (200 μ L, 4 mM/mouse). Mice in group C were injected intravenously with saline solution. Mice in group D were not treated and were used as a control. Mice in groups A-C were irradiated with NIR laser at 3 W/cm² for 2 min 24 h after injection. The mice were euthanized at 24 h after laser treatment, and tumors were removed, snap frozen, and cryosectioned into 1,000- μ m sections. The slides were stained with hematoxylin-eosin and examined under a Zeiss Axio Observer.Z1 fluorescence microscope (Carl Zeiss AG, Oberkochen, Germany). The images were captured by a Zeiss AxioCam MRc5 color camera, and the extent of tumor necrosis, expressed as a percentage of the entire tumor area, was analyzed with Zeiss AxioVision software (version 4.6.3).

Statistical analysis. All data were analyzed using a two-tailed Student *t*-test. The cytotoxicity of the nanoparticles was analyzed by using one-way ANOVA, followed by the post-hoc Tukey test (Graphpad Prism version 5.02; GraphPad Software, La Jolla, CA).

Supporting Information

The Supporting Information is available free of charge on the ACS Publications website.

Supplementary tables and figures are provided.

NOTES

The authors declare no conflicts of interest.

ACKNOWLEDGMENTS

We thank Kathryn Hale at the Department of Scientific Publications, MD Anderson Cancer Center for editing the manuscript. This work was supported in part by the John S. Dunn Foundation, by John S. Dunn, Sr. Distinguished Chair in Diagnostic Imaging to Dr. William A. Murphy Jr., and by the University Cancer Foundation via the Institutional Research Grant program at the University of Texas MD Anderson Cancer Center. This research was also conducted at the MD Anderson Center for Advanced Biomedical Imaging in-part with equipment support from General Electric Healthcare. The Research Animal Support Facility, Research Cyclotron Facility, NMR Core Facility, and Small Animal Imaging Facility are supported by a Cancer Center Support Grant from the National Institutes of Health (P30CA016672).

REFERENCES

- (1) Li, C. (2014) A targeted approach to cancer imaging and therapy. *Nat. Mater.* *13*, 110-115.
- (2) Zhou, M., Ku, G., Pagon, L., and Li, C. (2014) Theranostic probe for simultaneous in vivo photoacoustic imaging and confined photothermal ablation by pulsed laser at 1064 nm in 4T1 breast cancer model. *Nanoscale* *6*, 15228-15235.
- (3) Zhou, M., Li, J., Liang, S., Sood, A. K., Liang, D., and Li, C. (2015) CuS nanodots with ultrahigh efficient renal clearance for positron emission tomography imaging and image-guided photothermal therapy. *ACS Nano* *9*, 7085-7096.
- (4) Zhou, M., Tian, M., and Li, C. (2016) Copper-based nanomaterials for cancer imaging and therapy. *Bioconjug. Chem.* *27*, 1188-1199.
- (5) Zhou, M., Zhang, R., Huang, M., Lu, W., Song, S., Melancon, M. P., Tian, M., Liang, D., and Li, C. (2010) A chelator-free multifunctional [⁶⁴Cu]CuS nanoparticle platform for simultaneous micro-PET/CT imaging and photothermal ablation therapy. *J. Am. Chem. Soc.* *132*, 15351-15358.
- (6) Huang, J., Zhou, J., Zhuang, J., Gao, H., Huang, D., Wang, L., Wu, W., Li, Q., Yang, D.-P., and Han, M.-Y. (2017) Strong near-infrared absorbing and biocompatible CuS nanoparticles for rapid and efficient photothermal ablation of gram-positive and -negative bacteria. *ACS Appl. Mater. Interfaces* *9*, 36606-36614.
- (7) Zhang, W., Xiao, J., Cao, Q., Wang, W., Peng, X., Guan, G., Cui, Z., Zhang, Y., Wang, S., Zou, R., Wan, X., Qiu, H., and Hu, J. (2018) An easy-to-fabricate clearable CuS-superstructure-based multifunctional theranostic platform for efficient imaging guided chemo-photothermal therapy. *Nanoscale* *10*, 11430-11440.

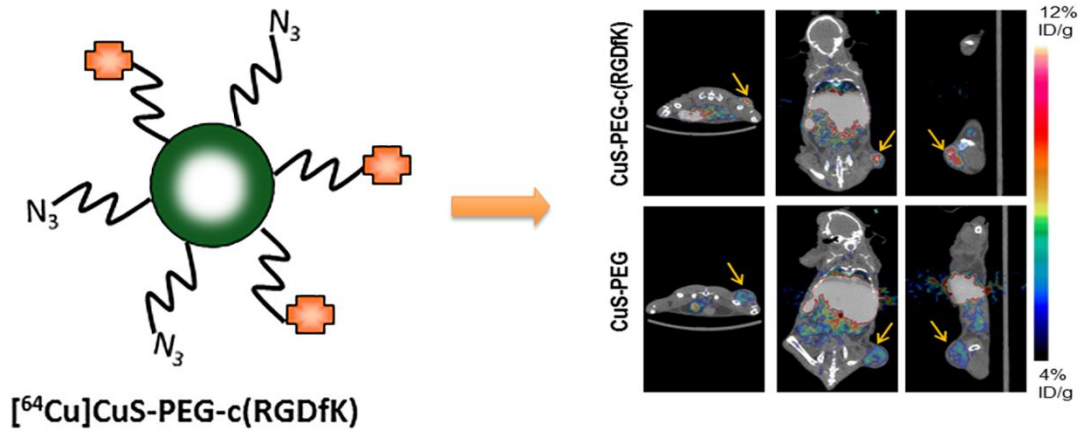
- 1
2
3 (8) Zhou, M., Chen, Y., Adachi, M., Wen, X., Erwin, B., Mawlawi, O., Lai, S. Y., and Li, C.
4
5 (2015) Single agent nanoparticle for radiotherapy and radio-photothermal therapy in
6
7 anaplastic thyroid cancer. *Biomaterials* 57, 41-49.
8
9
10 (9) Zhou, M., Zhao, J., Tian, M., Song, S., Zhang, R., Gupta, S., Tan, D., Shen, H., Ferrari,
11
12 M., and Li, C. (2015) Radio-photothermal therapy mediated by a single compartment
13
14 nanoplatform depletes tumor initiating cells and reduces lung metastasis in the orthotopic
15
16 4T1 breast tumor model. *Nanoscale* 7, 19438-19447.
17
18
19 (10) Goel, S., Chen, F., and Cai, W. (2014) Synthesis and biomedical applications of copper
20
21 sulfide nanoparticles: from sensors to theranostics. *Small* 10, 631-645.
22
23
24 (11) Blanco, E., Shen, H., and Ferrari, M. (2015) Principles of nanoparticle design for
25
26 overcoming biological barriers to drug delivery. *Nat. Biotechnol.* 33, 941-951.
27
28
29 (12) Davis, C. D., Emenaker, N. J., and Milner, J. A. (2010) Cellular proliferation, apoptosis
30
31 and angiogenesis: molecular targets for nutritional preemption of cancer. *Semin. Oncol.*
32
33 37, 243-257.
34
35
36 (13) Hood, J. D., and Cheresch, D. A. (2002) Role of integrins in cell invasion and migration.
37
38 *Nat. Rev. Cancer* 2, 91-100.
39
40 (14) Li, L., Wartchow, C. A., Danthi, S. N., Shen, Z., Dechene, N., Pease, J., Choi, H. S.,
41
42 Doede, T., Chu, P., Ning, S., Lee, D. Y., Bednarski, M. D., and Knox, S. J. (2004) A
43
44 novel antiangiogenesis therapy using an integrin antagonist or anti-Flk-1 antibody coated
45
46 ⁹⁰Y-labeled nanoparticles. *Int. J. Radiat. Oncol. Biol. Phys.* 58, 1215-1227.
47
48
49 (15) Ruoslahti, E. (1996) RGD and other recognition sequences for integrins. *Annu. Rev. Cell*
50
51 *Dev. Biol.* 12, 697-715.
52
53
54
55
56
57
58
59
60

- 1
2
3 (16) Lu, W., Melancon, M. P., Xiong, C. Y., Huang, Q., Elliott, A., Song, S. L., Zhang, R.,
4 Flores, L. G., Gelovani, J. G., Wang, L. H. V., Ku, G., Stafford, R. J., and Li, C. (2011)
5 Effects of photoacoustic imaging and photothermal ablation therapy mediated by targeted
6 hollow gold nanospheres in an orthotopic mouse xenograft model of glioma. *Cancer Res.*
7 *71*, 6116-6121.
8
9
10
11
12
13
14 (17) Wang, W., Ke, S., Wu, Q.-P., Charnsangavej, C., Gurfinkel, M., Gelovani, J. G.,
15 Abbruzzese, J. L., Sevick-Muraca, E. M., and Li, C. (2004) Near-infrared optical imaging
16 of integrin avb3 in human tumor xenografts. *Mol. Imaging* *3*, 343-351.
17
18
19
20
21 (18) Wang, W., McMurray, J. S., Wu, Q., Campbell, M. L., and Li, C. (2005) Convenient
22 solid-phase synthesis of diethylenetriaminepenta-acetic acid (DTPA)- conjugated cyclic
23 RGD peptide analogues. *Cancer Biother. Radiopharm.* *20*, 547-556.
24
25
26
27
28 (19) Lu, J., Shi, M., and Shoichet, M. S. (2009) Click chemistry functionalized polymeric
29 nanoparticles target corneal epithelial cells through RGD-cell surface receptors.
30
31
32 *Bioconjug. Chem.* *20*, 87-94.
33
34
35 (20) McCusker, C. F., Kocienski, P. J., Boyle, F. T., and Schatzlein, A. G. (2002) Solid-phase
36 synthesis of c(RGDfK) derivatives: on-resin cyclisation and lysine functionalisation.
37
38 *Bioorg. Med. Chem. Lett.* *12*, 547-549.
39
40
41
42 (21) Mindt, T. L., Muller, C., Stuker, F., Salazar, J. F., Hohn, A., Mueggler, T., Rudin, M.,
43 and Schibli, R. (2009) A "click chemistry" approach to the efficient synthesis of multiple
44 imaging probes derived from a single precursor. *Bioconjug. Chem.* *20*, 1940-1949.
45
46
47
48 (22) Xie, H., Diagaradjane, P., Deorukhkar, A. A., Goins, B., Bao, A., Phillips, W. T., Wang,
49 Z., Schwartz, J., and Krishnan, S. (2011) Integrin alphavbeta3-targeted gold nanoshells
50
51
52
53
54
55
56
57
58
59
60

1
2
3 augment tumor vasculature-specific imaging and therapy. *Int. J. Nanomedicine*. 6, 259-
4
5 269.
6

- 7
8 (23) Wilhelm, S., Tavares, A. J., Dai, Q., Ohta, S., Audet, J., Dvorak, H. F., and Chan, W. C.
9
10 W. (2016) Analysis of nanoparticle delivery to tumours. *Nature Rev. Mater.* 1, 16014.
11
12 (24) von Maltzahn, G., Ren, Y., Park, J. H., Min, D. H., Kotamraju, V. R., Jayakumar, J.,
13
14 Fogal, V., Sailor, M. J., Ruoslahti, E., and Bhatia, S. N. (2008) In vivo tumor cell
15
16 targeting with "click" nanoparticles. *Bioconjug. Chem.* 19, 1570-1578.
17
18
19
20
21
22
23
24
25
26
27
28
29
30
31
32
33
34
35
36
37
38
39
40
41
42
43
44
45
46
47
48
49
50
51
52
53
54
55
56
57
58
59
60

TOC graphic



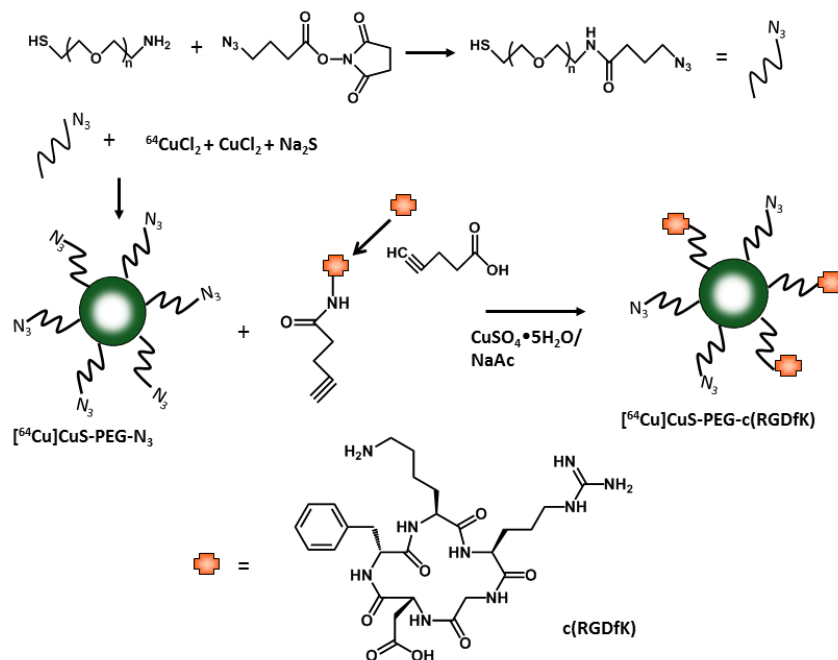


Figure 1. Schematic illustration of the synthesis of $[\text{}^{64}\text{Cu}]\text{CuS-PEG-c(RGDfK)}$ nanoparticles.

254x190mm (96 x 96 DPI)

Figure 2

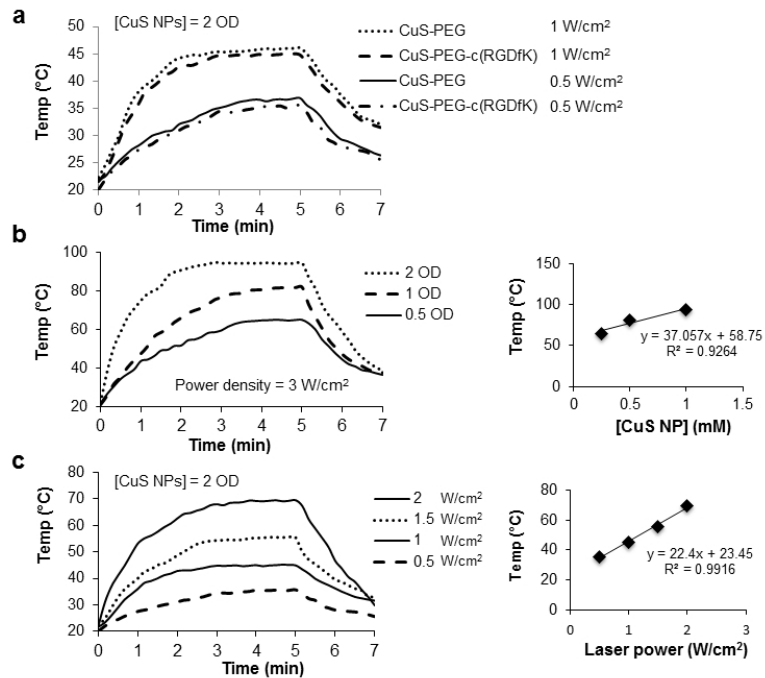


Figure 2. CuS-PEG-c(RGDfK) nanoparticles mediated efficient photothermal effects. (a) Comparison of the photothermal effects of CuS-PEG and CuS-PEG-c(RGDfK) nanoparticles in aqueous solution. (b) Photothermal effects of CuS-PEG-c(RGDfK) at different concentrations. (c) Photothermal effects of CuS-PEG-c(RGDfK) nanoparticles with different levels of laser power.

254x190mm (96 x 96 DPI)

Figure 3

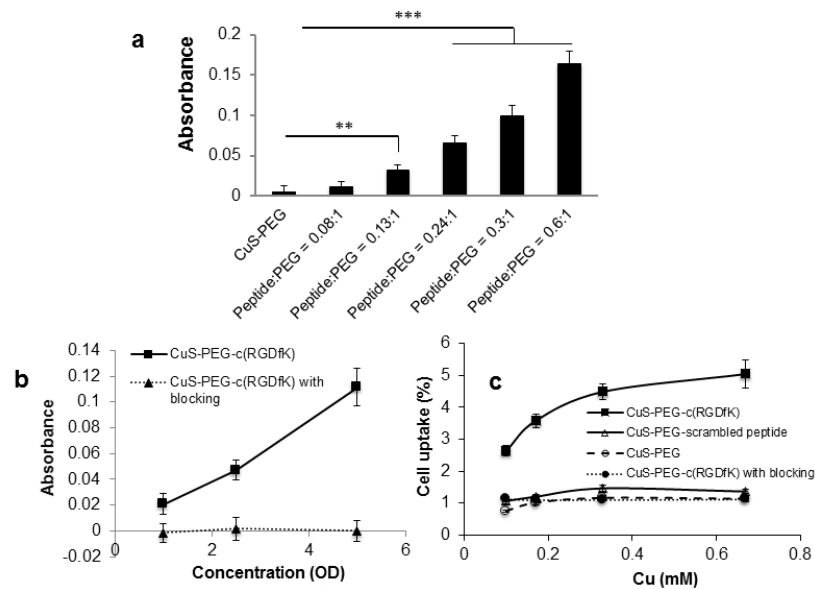


Figure 3. CuS-PEG-c(RGDfK) nanoparticles selectively bound to integrin $\alpha v \beta 3$ in vitro. (a) The binding affinity of CuS-PEG-c(RGDfK) nanoparticles at different concentrations on an integrin-coated plate using a sandwich ELISA ($n=3$); $*p<0.05$, $**p<0.01$. (b) Comparison of the binding affinities of CuS-PEG-c(RGDfK) nanoparticles and CuS-PEG-c(RGDfK) nanoparticles blocked with an excess amount of free c(RGDfK) peptide on an integrin-coated plate using a sandwich ELISA ($n=3$). (c) Cellular uptake of $[^{64}\text{Cu}]\text{CuS-PEG}$ and $[^{64}\text{Cu}]\text{CuS-PEG-c(RGDfK)}$ nanoparticles in U87 cells ($n=6/\text{group}$).

254x190mm (96 x 96 DPI)

Figure 4

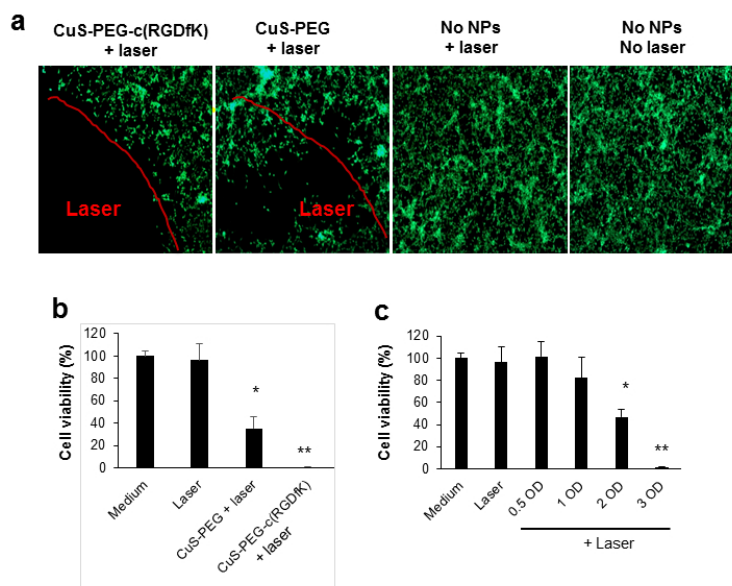


Figure 4. Visualization and quantification of U87 cell ablation after NIR laser treatment in vitro. (a) Photothermal ablation of U87 cells using NIR laser mediated by CuS-PEG-c(RGDfK) or CuS-PEG nanoparticles (NPs). Representative images are shown. Viable U87 cells were stained green. (b) Cell viability after treatment with the same concentration of CuS-PEG-c(RGDfK) or CuS-PEG nanoparticles (1.5 mM) and the same laser power ($n=5$ /group). (c) Cell viability after treatment with different concentrations (0.25-1.5 mM) of CuS-PEG-c(RGDfK) nanoparticles ($n=5$ /group; * $p<0.05$, ** $p<0.01$ compared to blank control).

254x190mm (96 x 96 DPI)

Figure 5

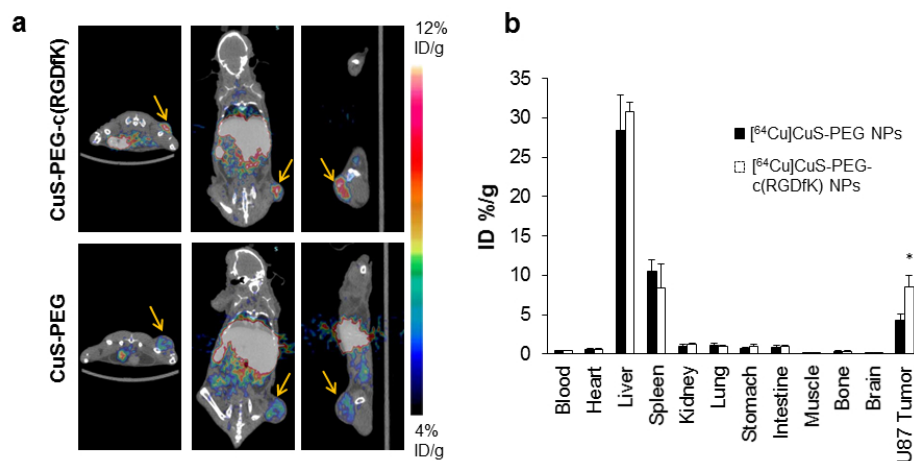


Figure 5. c(RGDfK)-tagged CuS nanoparticles increased the tumor-targeting efficiency over untagged nanoparticles. (a) PET/CT images of representative nude mice bearing a U87 xenograft tumor. Images were acquired 24 h after intravenous injection of [⁶⁴Cu]CuS-PEG-c(RGDfK) or [⁶⁴Cu]CuS-PEG nanoparticles. The arrows point to the tumor. (b) Biodistribution of [⁶⁴Cu]CuS-PEG and [⁶⁴Cu]CuS-PEG-c(RGDfK) nanoparticles (NPs) 24 h after intravenous administration of nanoparticles (n=4/group; p<0.05).

254x190mm (96 x 96 DPI)

Figure 6

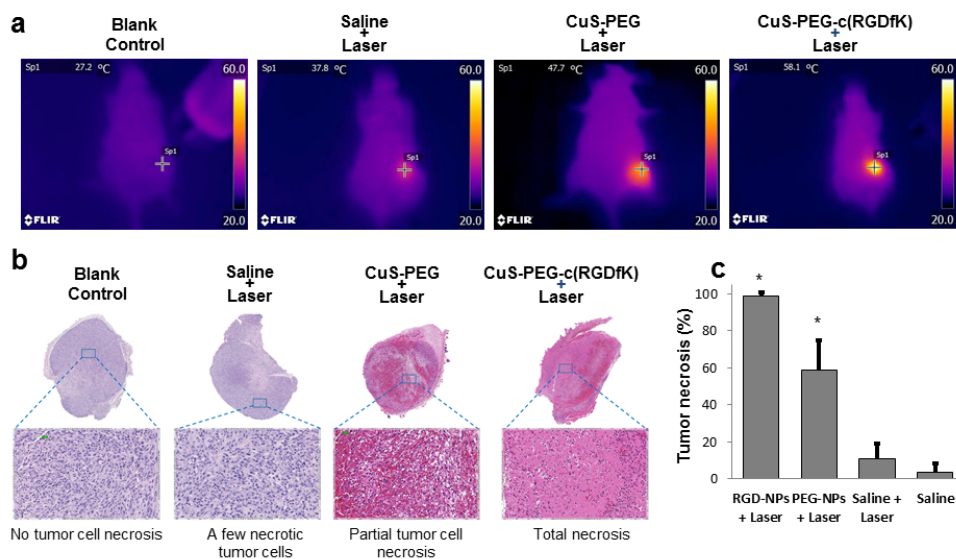


Figure 6. c(RGDfK)-tagged CuS nanoparticles mediated effective photothermal ablation of tumors in U87 xenograft-bearing mice. (a) Temperature at the tumor site during photothermal ablation study. (b) Representative microphotographs of histologic sections of tumors removed 24 h after photothermal ablation. (c) Quantitative analysis of the percentage of necrosis induced by different treatments; NPs, nanoparticles. NIR laser treatment was instituted for 3 min at a power density of 4 W/cm².

254x190mm (96 x 96 DPI)